Inorganic Chemistry

Article

pubs.acs.org/IC

Mono- and Dinuclear Cationic Iridium(III) Complexes Bearing a 2,5-Dipyridylpyrazine (2,5-dpp) Ligand

Loïc Donato,[†] Catherine E. McCusker,[‡] Felix N. Castellano,*[,‡] and Eli Zysman-Colman*[,†,§]

[†]Département de Chimie, Université de Sherbrooke, 2500 Boul. de l'Université, Sherbrooke, QC, Canada J1K 2R1

[‡]Department of Chemistry and Center for Photochemical Sciences, Bowling Green State University, Bowling Green, Ohio 43403, United States

Supporting Information

ABSTRACT: The synthesis, X-ray structures, photophysical, and electrochemical characterization of mono- (**1**) and dinuclear (**2**) cationic iridium(III) complexes bearing a 2,5-dipyridylpyrazine (2,5-dpp) ancillary ligand are reported. Upon the complexation of a first equivalent of iridium, the photoluminescence shifts markedly into the deep red (λ_{em} = 710 nm, Φ_{PL} = 0.9%) compared to other cationic iridium complexes such as $[Ir(ppy)_2(bpy)]PF_6$. With the coordination of a second equivalent of iridium, room temperature luminescence is completely quenched. Both **1** and **2** are luminescent at low temperatures but with distinct excited state decay kinetics; the emission of **2** is significantly red-shifted compared to **1**. Emission both at 298 and 77 K results from a mixed charge-transfer state. Density functional theory (DFT) calculations and electrochemical behavior point to an electronic communication between the two iridium complexes.

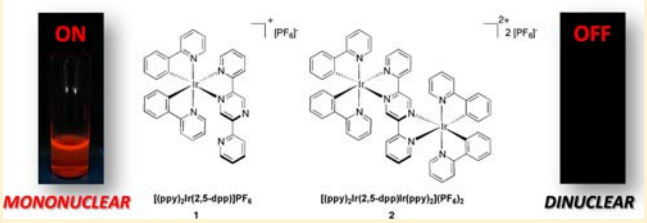

INTRODUCTION

Over the past decade, cationic iridium(III) complexes have received increasing attention because of their use as luminophoric materials in a wide variety of applications including light-emitting electrochemical cells (LEECs),[1] biolabeling agents,[2] chemosensors,[3] and as photocatalysts for solar fuels[4] and in organic transformations.[5] In the great majority of these cases, the luminophore used is a mononuclear heteroleptic complex. Far less explored are materials based on discrete oligohomonuclear complexes, most of the examples of which link the metal centers through a polyacene-type bridge.[6] In fact, to the best of our knowledge only a single example of a dinuclear cationic complex incorporating a π-conjugated bridging ligand, a 3,8-dipyridyl-4,7-phenanthroline,[6d] has been reported.

The ligand 2,5-dipyridylpyrazine (2,5-dpp) has had a long and storied past as a strong π-acceptor σ-donating bis(chelate), particularly involving Ru(II).[7] Indeed as a result of their properties, the use of 2,5-dpp and other related diazine ligands results in more photostable complexes.[8] Given our interest in the optoelectronic properties of multimetallic cationic iridium(III) complexes,[6m,t] we targeted complexes **1** and **2** for study, the first examples of iridium(III) complexes incorporating a 2,5-dpp ancillary ligand (Chart 1). We report here the improved synthesis of 2,5-dpp along with **1** and **2**, X-ray structures of the complexes, and their optoelectronic characterization.

Chart 1. Ir(III) Complexes under Investigation in This Study

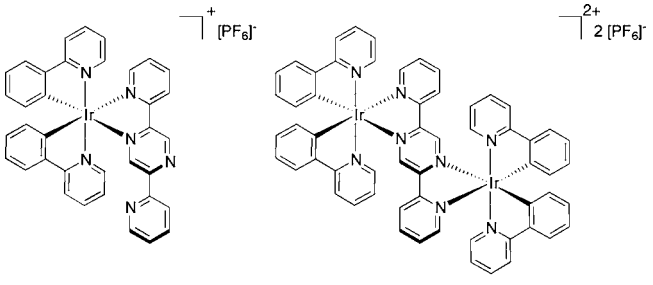

EXPERIMENTAL SECTION

General Procedures. Commercial chemicals were used as supplied. All reactions were performed using standard Schlenk techniques under an inert (N_2) atmosphere. All experiments were carried out with freshly distilled anhydrous solvents obtained from a Pure Solv solvent purification system from Innovative Technologies except where specifically mentioned. Flash column chromatography was performed using silica gel (Silia-P from Silicycle, 60 Å, 40−63 μm). Analytical thin layer chromatography (TLC) was performed with silica plates with aluminum backings (250 μm with indicator F-254). Compounds were visualized under UV light. ^{1}H, ^{19}F, and ^{13}C NMR spectra were recorded on a Varian INOVA spectrometer at 400 MHz, 376 and 100 MHz respectively. The following abbreviations have been used for multiplicity assignments: "s" for singlet, "d" for doublet, "t" for triplet, "m" for multiplet. One of deuterated acetonitrile (CD_3CN), deuterated chloroform ($CDCl_3$) or deuterated acetone (acetone-d_6) was used as the solvent of record. Trifluoroacetic acid (TFA) was used as the reference for ^{19}F NMR. Spectra were referenced to the solvent

Received: February 22, 2013
Published: July 18, 2013

   dx.doi.org/10.1021/ic400478d | Inorg. Chem. 2013, 52, 8495−8504

peak. Exact mass measurements were performed on a quadrupole time-of-flight (ESI-Q-TOF), model Maxis from Bruker in positive electrospray ionization mode, and spectra were recorded at the Université de Sherbrooke.

Synthesis. *2,5-Di(pyridin-2-yl)pyrazine, 2,5-dpp.* To a suspension of 2-bromopyridine (9.25 mmol, 880 μL, 2.2 equiv.) in 30 mL of dry THF under a N_2 atmosphere at −78 °C was added dropwise over 30 min *n*-BuLi (9.25 mmol, 5.8 mL, 2.2 equiv.). The reaction was stirred for 30 min, and a mixture of $ZnCl_2$ (1.25 g, 9.25 mmol, 2.2 equiv.) in 30 mL of dry THF was added via cannula. The mixture was then stirred 2 h at room temperature (RT) and then added via cannula to a mixture of 2,5-dibromopyrazine, 2,5-diBrpyz, (1.00 g, 4.20 mmol, 1.0 equiv.) and $Pd(PPh_3)_4$ (485 mg, 10 mol %) in 40 mL of dry THF at RT. The reaction mixture was stirred overnight at 65 °C under nitrogen. The solid was filtered, washed several times with diethyl ether, and dissolved in 100 mL of saturated aqueous EDTA and 50 mL of saturated aqueous Na_2CO_3. The mixture was stirred for 1 h and the solid was filtered, washed several times with water and dried over reduced pressure to obtain a beige solid (550 mg) that was analytically pure.

Beige solid. Yield: 55%. R_f: 0.25 (DCM/Acetone 90/10; Silica). Mp: 186−190 °C (lit:[7a] 226−227 °C) . ^{1}H NMR (400 MHz, CD_3CN) δ (ppm): 9.66 (s, 1H), 8.76 (d, J = 4.8 Hz, 1H), 8.45 (d, J = 8.0 Hz, 1H), 7.98 (td, J = 7.6, 1.6 Hz, 1H), 7.49 (dd, J = 7.6, 4.4 Hz, 1H). ^{13}C NMR (100 MHz, $CDCl_3$) δ (ppm): 154.5, 150.7, 149.8, 142.2, 137.3, 124.6, 121.9. HR-MS (ES-Q-TOF) ($C_{14}H_{11}N_4Na^+$) Calculated: 257.0798; Experimental: 257.0800. The compound characterization is in agreement with that previously reported.[9]

*Iridium(III) Bis[2-phenylpyridine-N,C2′]-2,5-di(pyridin-2-yl)-pyrazine Hexafluorophosphate, [(ppy)$_2$Ir(**2,5-dpp**)](PF$_6$), **1**.* 2-Phenylpyridine, ppyH, (30 μL, 0.20 mmol, 2.2 equiv.) was mixed with $IrCl_3{\cdot}6H_2O$ (32 mg, 0.093 mmol, 1.0 equiv.) in a mixture of 2-ethoxyethanol and water (6/1 v/v) to reach a concentration in $IrCl_3{\cdot}6H_2O$ of 0.04 M. The mixture was degassed by multiple vacuum and N_2 purging cycles. The suspension was heated at 130 °C for 24 h. A yellow precipitate formed during the reaction and was filtered. To this solid was added **2,5-dpp** (55 mg, 0.233 mmol, 2.5 equiv.) and 2-ethoxyethanol to reach a concentration in iridium of 0.04 M. The mixture was degassed by multiple vacuum and N_2 purging cycles. The suspension was heated at 130 °C for 24 h. The reaction mixture was cooled to RT and diluted with water. The aqueous suspension was washed several times with Et_2O. The aqueous layer was heated at 70 °C for 30 min and cooled back down to RT. A solution of NH_4PF_6 (10 equiv., 1.0 g/10 mL) was added to the aqueous phase, which caused the precipitation of a red solid. The suspension was cooled to 0 °C for 1 h, filtered, and the resulting solid was washed with water. The crude solid was purified by flash chromatography on silica gel using DCM + 5% NEt_3 to DCM/Acetone (9/1) + 5% NEt_3.

Red solid. Mp: 245−250 °C. Yield: 80%. R_f: 0.20 (DCM/Acetone 90/10; Silica). ^{1}H NMR (400 MHz, acetone-d_6) δ (ppm): 10.09 (d, J = 1.2 Hz, 1H), 9.13 (d, J = 1.2 Hz, 1H), 9.08 (d, J = 8.0 Hz, 1H), 8.56 (m, 1H), 8.45 (dt, J = 8.0, 1.2 Hz, 1H), 8.38 (td, J = 8.0, 1.6 Hz, 1H), 8.25 (t, J = 9.6 Hz, 2H), 8.15 (m, 2H), 7.91−8.03 (m, 5H), 7.85 (d, J = 5.6 Hz, 1H), 7.80 (dd, J = 8.0, 5.6, 1.2 Hz, 1H), 7.51 (ddd, J = 7.6, 4.8, 1.2 Hz, 1H), 7.04−7.18 (m, 4H), 6.93−7.01 (m, 2H), 6.41 (dd, J = 7.6, 0.8 Hz, 1H), 6.33 (dd, J = 7.6, 0.8 Hz, 1H). ^{19}F NMR (376 MHz, acetone-d_6) δ (ppm): 72.34 (d, J = 706 Hz). HR-MS (ES-Q-TOF) ($C_{36}H_{26}N_6Ir^+$) Calculated: 735.1848; Experimental: 735.1882.

*Iridium(III) [μ-2,5-di(pyridin-2-yl)pyrazine-N^1,N^2:N^3,N^4] tetrakis(2-phenylpyridine-N,C2′)di-Bis[hexafluorophosphate], [(ppy)$_2$Ir(**2,5-dpp**)Ir(ppy)$_2$](PF$_6$)$_2$, **2**.* 2-Phenylpyridine, ppyH, (105 μL, 0.739 mmol, 13.2 equiv.) was mixed with $IrCl_3{\cdot}6H_2O$ (118 mg, 0.336 mmol, 6.00 equiv.) in a mixture of 2-ethoxyethanol and water (6/1 v/v) to reach a concentration in $IrCl_3{\cdot}6H_2O$ of 0.04 M. The mixture was degassed by multiple vacuum and N_2 purging cycles. The suspension was heated at 130 °C for 24 h. A yellow precipitate formed during the reaction and was filtered. To this solid was added **2,5-dpp** (13 mg, 0.056 mmol, 1.0 equiv.) and 2-ethoxyethanol to reach a concentration in iridium of 0.04 M. The mixture was degassed by multiple vacuum and N_2 purging cycles. The suspension was heated at 130 °C for 24 h. The reaction mixture was cooled to RT and diluted with water. The aqueous suspension was washed several times with Et_2O. The aqueous layer was heated at 70 °C for 30 min and cooled back down to RT. A solution of NH_4PF_6 (20 equiv., 1.0 g/10 mL) was added to the aqueous phase to cause the precipitation of a green solid. The suspension was cooled to 0 °C for 1 h, filtered, and the resulting solid was washed with water. The crude solid was purified by flash chromatography on silica gel using 5% NEt_3/DCM followed by 5% NEt_3/DCM/Acetone (9/1).

Green solid. Mp: 258−262 °C. Yield: 56%. R_f: 0.20 (DCM/Acetone 90/10; Silica). ^{1}H NMR (400 MHz, Acetone D_6) δ (ppm): 9.23 (s, 0.3H), 9.14 (s, 1.0H), 8.31−8.20 (m, 4.9H), 8.14 (d, J = 5.2 Hz, 1.0H), 8.13−7.89 (m, 7.0H), 7.83−7.78 (m, 1.4H), 7.69 (d, J = 5.6 Hz, 0.3H), 7.65 (d, J = 5.6 Hz, 1.0H), 7.28−6.99 (m, 6.4H), 6.50 (d, J = 7.2 Hz, 1.0H), 6.90−6.96 (m, 1.6H), 6.50 (d, J = 7.2 Hz, 1H), 6.40 (d, J = 7.2 Hz, 0.3H), 6.23 (d, J = 7.2 Hz, 0.3H), 6.19 (d, J = 7.2 Hz, 1.0H). ^{19}F NMR (376 MHz, acetone-d_6) δ (ppm): −72.98 (d, J = 706 Hz). HR-MS (ES-Q-TOF) ($C_{58}H_{42}N_8Ir^{2+}$) Calculated: 617.1379\; Experimental: 617.1400.

Steady-State Photophysical Measurements. All absorption samples were prepared in HPLC grade acetonitrile (ACN) with varying concentrations on the order of μM. Absorption spectra were recorded at RT using a Shimadzu UV-1800 double beam spectrophotometer. Molar absorptivity determination was verified by linear least-squares fit of values obtained from at least three independent solutions at varying concentrations ranging from 5.50 to 145 μM. The absorption spectra for **2** were obtained from a diastereomeric mixture. Optically dilute (OD ∼0.1−0.2) solutions for RT emission and quantum yield experiments were prepared in spectrophotometric grade ACN, and solutions for low temperature emission experiments were prepared in anhydrous 2-methyl-tetrahydrofuran (2-MeTHF). Solutions were degassed with argon for ∼20 min before measurements. Steady state emission spectra were collected with a FL/FS920 fluorometer (Edinburgh Instruments) equipped with a 450 W Xe arc lamp as the excitation source. The emission signal was detected with a Peltier-cooled, red-sensitive PMT (R2658P Hamamatsu). Low temperature spectra were collected using an Optistat-DN optical cryostat and ITC-503 temperature controller (Oxford Instruments). Samples were allowed to equilibrate for 30 min at 77 K before each measurement. The quantum yield of **1** was measured relative to $[Ru(bpy)_3](PF_6)_2$ in aerated acetonitrile (Φ = 0.018).[10]

Time-Resolved Photophysical Measurements. Optically dilute (OD ∼ 0.1−0.2) solutions for time-resolved emission and transient absorption experiments were prepared in spectrophotometric grade ACN and solutions for low temperature emission experiments were prepared in anhydrous 2-MeTHF. Solutions were degassed with argon for ∼20 min before measurements. Time-resolved emission and transient absorption data were collected with an LP920 laser flash photolysis system (Edinburgh Instruments). The excitation source was the Vibrant LD 355 II Nd:YAG/OPO system (OPOTEK). Data acquisition was controlled by the LP900 software program (Edinburgh Instrument). Kinetic traces were collected with a PMT (R928 Hamamatsu), and emission and transient absorption spectra were collected with an iStar ICCD camera (Andor Technology). Low temperature emission spectra were collected using an Optistat-DN optical cryostat and ITC-503 temperature controller (Oxford Instruments). Samples were allowed to equilibrate for 30 min at 77 K before each measurement. Kinetic traces were fit with single or double exponential functions using IGOR Pro.

Electrochemistry. Cyclic voltammetry (CV) measurements for **1** and **2** were performed on an Electrochemical Analyzer potentiostat model 600D from CH Instruments. The CV data collected for **2** were from a diastereomeric mixture. Solutions for CV were prepared in acetonitrile (ACN), distilled over P_2O_5 with tetra-*n*-butylammonium hexafluorophosphate ($TBAPF_6$; about 0.1 M in ACN) added as the supporting electrolyte. The concentration of the samples was about 1 mM and ACN-saturated nitrogen bubbling for about 15 min occurred prior to scanning and electrochemical measurements were performed in a glass cell under a nitrogen atmosphere. A nonaqueous Ag^+/Ag

dx.doi.org/10.1021/ic400478d | Inorg. Chem. 2013, 52, 8495−8504

Scheme 1. Synthesis of 2,5-dpp and Complexes 1 and 2

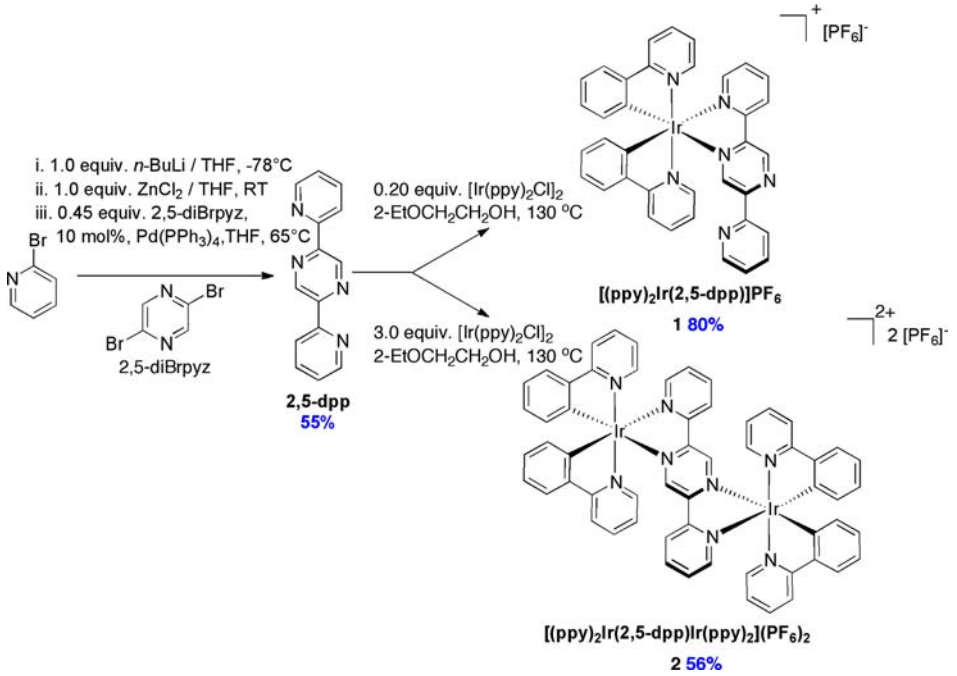

electrode (silver wire in a solution of 0.1 M $AgNO_3$ in ACN) was used as the pseudoreference electrode; a glassy-carbon electrode was used for the working electrode and a Pt electrode was used as the counter electrode. The redox potentials are reported relative to a saturated calomel electrode (SCE) with a ferrocenium/ferrocene (Fc^+/Fc) redox couple as an internal reference (0.380 V vs SCE).[11]

Computations. Density functional theory (DFT) calculations were performed with the Gaussian 09[12] suite. The level of theory for all DFT[13] and time-dependent DFT (TDDFT)[14] calculations was B3LYP; excited-state triplet geometries were calculated using the unrestricted B3LYP method (UB3LYP).[15] The 6-31G* basis set[16] was used for C, H, and N directly bonded to iridium while the other C, H, and N atoms where undertaken with 3-21G* basis set,[17] and the VDZ (valence double ζ) with SBKJC effective core potential basis set[17a,18] was used for iridium. The predicted phosphorescence wavelengths were obtained by energy difference between the triplet and singlet states at their respective optimized geometries.[19] The energy, oscillator strength, and related molecular orbital (MO) contributions for the 100 lowest singlet−singlet and 5 lowest singlet−triplet excitations were obtained from the TD-DFT/singlets and the TD-DFT/triplets output files, respectively. The calculated absorption spectra were visualized with GaussSum 2.1 (fwhm: 1000 cm^{-1}).[20] An ACN quantum mechanical continuum solvation model was employed throughout the computational study.[21]

RESULTS AND DISCUSSION

Ligand and Complex Synthesis. Bridging 2,5-dipyridylpyrazine (**2,5-dpp**) was obtained efficiently in 55% yield in a single-step through a Negishi cross coupling of 2-bromopyridine and 2,5-dibromopyrazine (2,5-diBrpyz), Scheme 1. This simple synthesis contrasts will the multistep and low-yielding condensation strategy commonly used in the literature.[7a,22]

Complexes **1** and **2** were obtained through a one-pot two-step reaction protocol previously used by us[23] wherein the $[(ppy)_2Ir(\mu\text{-}Cl)]_2$ dimer was not isolated. Mononuclear complex **1** was obtained in very good yield when an excess of **2,5-dpp** was employed. Dinuclear complex **2** was obtained in good yield as a mixture of diastereomers when **2,5-dpp** was used as the limiting reagent. Complexes **1** and **2** were characterized by ^1H and ^{19}F NMR, Mp, HPLC and HRMS analyses, and the X-ray structures of each were solved.

X-ray Structures. Complexes **1** and **2** each crystallized from slow diffusion of iPr_2O into an ACN solution of the complex. Suitable single crystals for X-ray analysis were obtained for **1** and **2**, and their molecular structures are shown in Figure 1 while refinement parameters are available in Supporting Information, Table S1. Both complexes crystallized within the $P\bar{1}$ space group and are triclinic. Complex **1** crystallized as dark purple plates as an ACN solvate in the asymmetric unit while **2** crystallized as dark green prisms also as an ACN solvate. In each case, the coordination environment of the iridium is that of a distorted octahedron with a mutually *trans*-configuration of the nitrogen atoms of the two pyridine rings of the ppy ligands. Selected bond lengths and bond and torsional angles are collected in Supporting Information, Tables S2−S3 and are similar to those of other heteroleptic iridium complexes such as $[Ir(ppy)_2(bpy)]PF_6$, where bpy = 2,2′-bipyridine.[24]

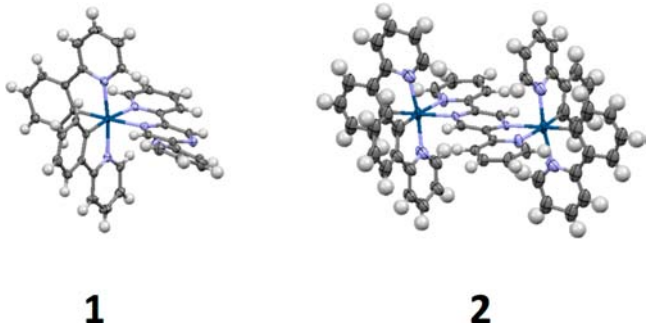

Figure 1. Perspective views of X-ray structures of **1** and the ΔΛ isomer of **2** (50% ellipsoid probabilities). Counterions (PF_6^-) and solvent molecules have been omitted for clarity.

In **1**, there is a small torsion between the coordinating pyridine and pyrazine rings (interplanar angle of 8.4°) as well as

dx.doi.org/10.1021/ic400478d | Inorg. Chem. 2013, 52, 8495−8504

a twisting of the noncoordinating pyridine ring of the 2,5-dpp ligand with an interplanar angle of 12.8°). Of note, the pyridine nitrogen atom is *trans* to the noncoordinating nitrogen atom of the pyrazine moiety, similar to that observed[9] for $[ZnCl_2(2,5\text{-dpp})(DMF)]$ while in the crystal structure of $[Ru(bpy)_2(2,5\text{-dpp})](PF_6)_2$ the tethered pyridine ring is disordered and these two nitrogen atoms are in some instances disposed in an *S-cis* conformation.[25] This deviation from planarity of the distal pyridine is probably due to the weak intermolecular π-stacking interaction between the noncoordinating pyridine rings in adjacent enantiomeric molecules evidenced by the slip-stack and face-to-face separation between their centroids of 3.806 Å (Supporting Information, Figure S1). Both Δ and Λ isomers are present in the lattice.

Complex **2** is C_2-symmetric, and crystallizes as the *meso* ΔΛ form, with the two iridium atoms separated by 6.996 Å and with each iridium atom located 0.118 Å above and below the mean plane of the 2,5-dpp ligand. This stereochemical arrangement in a dinuclear iridium complex has been previously reported.[6d,26] The $Ir_1\cdots Ir_2$ distance in **2** places the iridium subunits substantially further apart than the majority of the few other dinuclear and polynuclear iridium crystal structures reported to date.[6r,26,27] Exceptionally, recently several crystal structures of dinuclear iridium complexes have been solved wherein the nonbonded Ir···Ir distance ranges from 7.467 Å to 10.007 Å.[6d,f,h,28] As with **1**, there are distortions from planarity over the 2,5-dpp in **2** (interplanar angle between each of the pyridines and pyrazine of 8.14°).

Solution Structures. The ^{1}H NMR spectra of 2,5-dpp in CD_3CN and **1** and **2** in acetone-d_6 are shown in Figure 2. For **1**, the two ppy ligands are nonequivalent and thus each proton has its own resonance, exemplified by the two singlets of the pyrazine at 10.09 and 9.13 ppm. For **2**, there are two sets of ^{1}H NMR resonances, pointing to the presence of a diastereomeric mixture of *meso* ΛΔ and a racemic ΔΔ and ΛΛ in an about 3:1 ratio, indicating some degree of enrichment of one of the distereoisomers during purification, similar to that observed for a related 3,8-dipyridyl-4,7-phenanthroline-bridged dinuclear complex reported by Sauvage and co-workers.[6d]

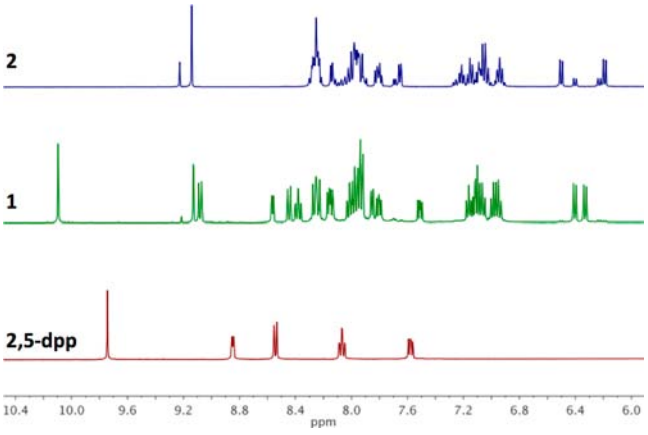

Figure 2. ^{1}H NMR spectra of **1** and **2** in acetone-d_6 and 2,5-dpp in ACN-d_3. The ^{1}H NMR of **2** shows a 3:1 mixture of diastereomers.

Electrochemistry. Cyclic voltammetry (CV) scans (Figure 3) were used to comprehend the electrochemical behavior and to determine the electrochemical gap (ΔE_{redox}) of **1** and **2**. The electrochemical data are given vs SCE and are listed in Table 1. During the anodic scan both complexes underwent irreversible

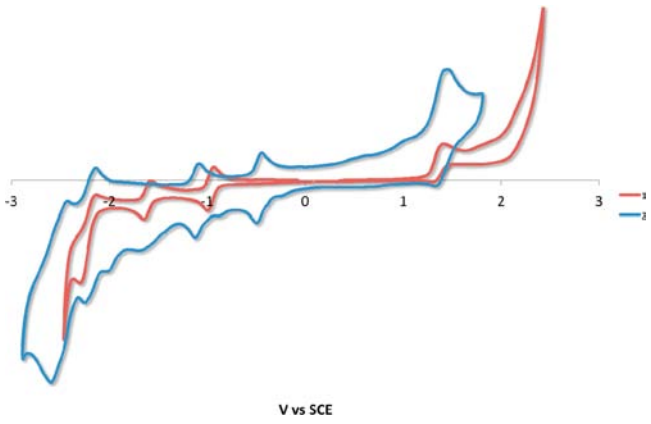

Figure 3. CVs of **1** (red) and **2** (blue) in N_2-saturated ACN at 298 K. Scan rate: 50 mV/s.

oxidations at 1.42−1.45 V. These first oxidations, assigned to involve the Ir^{III}/Ir^{IV} redox couple with significant ppy contribution, are shifted to far more positive potential compared to $[Ir(ppy)_2(bpy)]$ ($E^{ox}_{1/2}$ = 1.25 V) because of the electron withdrawing character of 2,5-dpp.[23] By contrast, the first oxidation of ruthenium analogue $[Ru(bpy)_2(2,5\text{-dpp})](PF_6)_2$ was reported[30] to be 1.67 V versus SCE, which is shifted cathodically compared to the first oxidation of about 1.39 V reported[7b,31] for $[Ru(bpy)_2(2,5\text{-dpp})Ru(bpy)_2](PF_6)_4$. However, similarly to **1** and **2**, the oxidations for both ruthenium 2,5-dpp complexes are shifted significantly to more positive potential compared to $[Ru(bpy)_3](PF_6)_2$ because of the existence of more electron deficient 2,5-dpp chelate versus bpy.[32]

The ΔE_p for the oxidation wave in **2** is 116 mV, implying a one-electron oxidation process. Given the conjugated nature of the bridging 2,5-dpp ligand in **2** and the high degree of metal−metal interactions with two observed oxidation processes in related $[Ru(bpy)_2(2,5\text{-dpp})Ru(bpy)_2](PF_6)_4$ ($E^{ox}_{1/2,2}$ = 1.58 V),[31] the absence of two discernible oxidation waves in **2** is more likely due to the presence of a second nonresolved oxidation wave in the CV than the result of an absence of electronic coupling between the two iridium atoms. Such a lack of resolution is surprising given that in other related polynuclear iridium systems, distinct and well separated oxidation processes are observed ($170 < \Delta E < 480$ mV) resulting from the sequential oxidation of each iridium center[6f−h,m,r,26,27,33] while systems with electronically decoupled iridium atoms separated frequently through polyacene bridging moieties show a single 2-eletron oxidation.[6a,l,34] However, from the DFT calculations (vide infra), the highest occupied molecular orbital (HOMO) and HOMO−1 have similar energies, which may explain the absence of resolved oxidation processes in **2**.

Upon cathodic sweep, **1** showed three quasi-reversible reduction waves separated by 680 and 570 mV, respectively. The first two reduction processes are assigned to successive one-electron reductions of the bridging 2,5-dpp ligand based on DFT calculations and similar electrochemical behavior to $[Ru(bpy)_2(2,5\text{-dpp})](PF_6)_2$.[31] Because of the increased conjugation of the 2,5-dpp compared to bpy, the first reduction process in **1** at −0.97 V is anodically shifted by 410 mV compared to $[Ir(ppy)_2(bpy)]PF_6$.[23] As a result of the large stabilization of the π^* orbitals of 2,5-dpp upon complexation with successive equivalents of "$[Ir(ppy)_2]^+$", its reduction

dx.doi.org/10.1021/ic400478d | Inorg. Chem. 2013, 52, 8495−8504

Table 1. Electrochemical Data of 1 and 2 (V vs. SCE) Obtained in ACN[a,b]

	E_{ox} / V	E_{red} /V (ΔE_p /mV)							
	E_{pa}	$E_{1/2,1}$	$E_{1/2,2}$	$E_{1/2,3}$	$E_{1/2,4}$	$E_{1/2,5}$	E_{HOMO}[c]/eV	E_{LUMO}[c]/eV	ΔE /V
1	1.42[d]	−0.97 (66)	−1.65 (71)	−2.22 (144)			−5.84	−3.42	2.32
2	1.45[d]	−0.47 (61)	−1.09 (55)	−1.50[d]	−1.98[d]	−2.19 (79)	−5.87	−3.92	1.92

[a]Conditions: ca. 1.5 mM of complex and nBu_4NPF_6 (ca. 0.1 M) in N_2-saturated ACN at 298 K; Scan rate: 50 mV/s. Potentials (V) are versus SCE (Fc/Fc^+ versus SCE = 0.38 V in ACN);[11] $\Delta E = \Delta E_{redox}$; $\Delta E_p = |E_{pa} - E_{pc}|$, where E_{pa} = anodic peak potential and E_{pc} = cathodic peak potential; [b]Reversible and pseudoreversible processes ($i_{pa}/i_{pc} > 0.9$) are reported as $E_{1/2} = (E_{pa} + E_{pc})/2$ and result from one-electron processes. [c]The HOMO and LUMO energies were calculated using the relation $E_{HOMO/LUMO} = -(E_{onset\ Ox./Red.\ vs\ Fc} + 4.8)$ eV.[29] [d]Irreversible: E_{pa} reported for oxidation potentials and E_{pc} reported for reduction potentials.

becomes much more facile[35] ($E_{red,1}$ for 2,5-dpp = −1.90 V vs SCE).[36] Indeed, the first two reduction waves in **2** are shifted to even more positive potential at −0.47 and −1.09 V, respectively, compared to **1**, implicating a significant stabilization of the lowest unoccupied molecular orbital (LUMO) upon the second complexation event. A corresponding 400 mV decrease in the electrochemical gap of **2** compared to **1** is thus observed. HOMO and LUMO levels inferred from CV measurements mirror well those determined by DFT calculations (**1**: E_{HOMO} = −5.86 eV, E_{LUMO} = −2.98 eV; **2**: E_{HOMO} = −6.00 eV, E_{LUMO} = −3.60 eV). A further three reduction processes are observed in **2** at more negative potentials. DFT calculations point to two successive reductions centered on the 2,5-dpp ligand in both **1** and **2**; the remaining reduction processes are predicted to also involve reduction of the ppy ligands.

Photophysical Characterization. The absorption and emission spectra for **1** and **2** are shown in Figures 4 and 5,

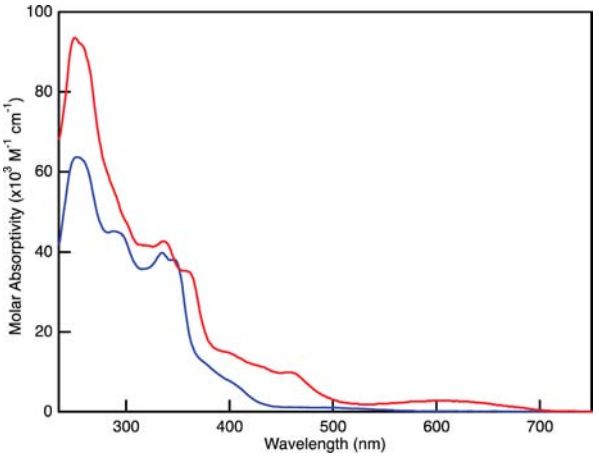

Figure 4. UV−visible absorption spectra of **1** (blue) and **2** (red) in ACN solution.

respectively, and pertinent photophysical data is summarized in Table 2. The RT absorption spectra for **1** and **2** exhibit similar gross features out too around 300 nm. The intensity of the high-energy bands, which correspond to predominantly ligand-centered (^{1}LC) $\pi-\pi^*$ transitions, in **2** are higher than those in **1**. Inspection of the absorption spectrum for $[Ir(ppy)_2(BPP)]$, where BPP = 2,2′:5′,2″-terpyridine, as recently reported by Vos and co-workers[37] suggests a blue-shifted absorption spectrum compared to **1**. Analogous to that observed for $[Ru(bpy)_2(2,5\text{-dpp})Ru(bpy)_2](PF_6)_4$ and $[Ru(bpy)_2(2,5\text{-dpp})](PF_6)_2$,[38] at longer wavelengths, the absorption spectrum in **2** is red-shifted compared to **1**. These lower-intensity bands are the result of mixed metal-to-ligand and ligand-to-ligand charger transfer

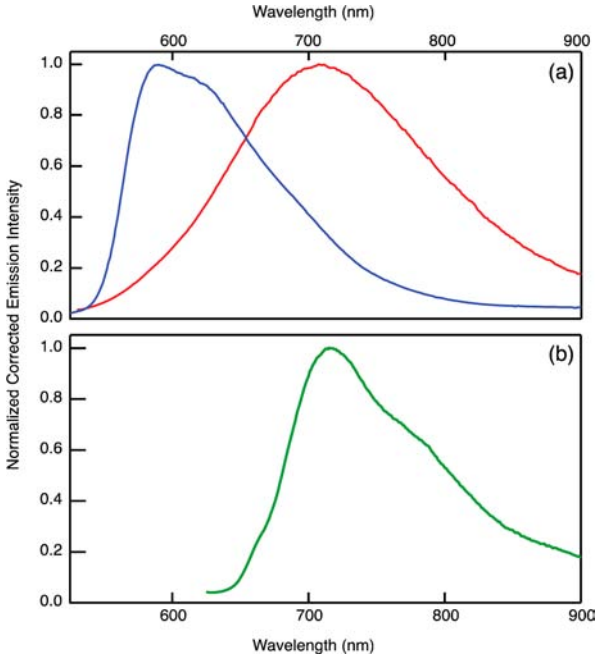

Figure 5. (a) Steady state emission spectra of **1**, resulting from 500 nm excitation, in acetonitrile at RT (red) and in 2-MeTHF at 77 K (blue). (b) Steady state emission spectrum of **2** with 600 nm excitation in 2-MeTHF at 77 K (green).

(^{1}MLCT/^{1}LLCT) transitions. There is the additional appearance of an unusual low-intensity feature (ε = 2492 M^{-1} cm^{-1}) centered at 606 nm in **2**.

The RT steady state emission spectrum of **1** is broad and featureless with an emission maximum at 710 nm. At low temperature, the emission shifts to higher energy (ΔE ∼2900 cm^{-1}) and becomes slightly more structured. This rigidochromic shift at low temperature is an indication of a significant excited state dipole moment, and suggests that the emissive state is charge transfer (CT) rather than ligand centered (LC) in nature.[39] This deep-red emission is distinctive by comparison to most other red-emitting (λ_{em}> 620 nm in ACN) complexes of the form $[Ir(ppy)_2(N^\wedge N)]^+$ given (i) the very low emission energy and (ii) the relatively nonconjugated nature or absence of electron-withdrawing groups decorating the ancillary ligand.[6m,8a,40] The photoluminescence (PL) quantum yield (Φ_{PL}) of around 1% is comparable to other Ir(III) red emitters. By contrast, **2** has no detectable emission at RT in the visible or near-infrared regions of the spectrum, but at low temperature a red and somewhat structured emission can be detected. Considering the significant red shift (∼125 nm, 2992 cm^{-1}) between the low temperature emission maxima of

dx.doi.org/10.1021/ic400478d | Inorg. Chem. 2013, 52, 8495−8504

Table 2. Spectroscopic and Photophysical Data for 1−2 in ACN

	λ_{abs} /nm[a] [ε /M^{-1} cm^{-1}]	λ_{em}/nm 298 K[a]	λ_{em}/nm 77 K[b]	τ_{em}/ns 298 K[a]	τ_{em}/ns 77 K[b]	Φ_{PL} /%[c]
1	252 [63724]; 290 [44276]; 334 [41103]; 375 [13000]; 460 [1281]	710	589	40 ± 5 (1.0) 240 ± 20 (0.02)[e,f] 40 ± 5 (1.0) 240 ± 50 (0.21) 1250 ± 200 (0.07)[g,h]	3560 ± 200	0.9 ± 0.15
2	250 [93534]; 337 [40055]; 360 [32847]; 390 [14454]; 457 [9198]; 606 [2492]	*d*	715	*d*	360 ± 30 (0.97)[e] 930 ± 60 (1.0)	*d*

[a]Measured in ACN solution at 298 K. [b]Measured in 2-MeTHF solution at 77 K. [c]Absolute quantum yield measured in ACN at 298 K, relative quantum yield measured in ACN at 298 K using aerated $[Ru(bpy)_3](PF_6)_2$ as the standard (Φ_{PL} = 0.018).[10] [d]No detectable emission. [e]Biexponential emission decay (relative contribution). [f]Emission decay at 700 nm. [g]Sum of three single exponential functions for the emission decay (relative contribution). [h]Emission decay measured at 600 nm.

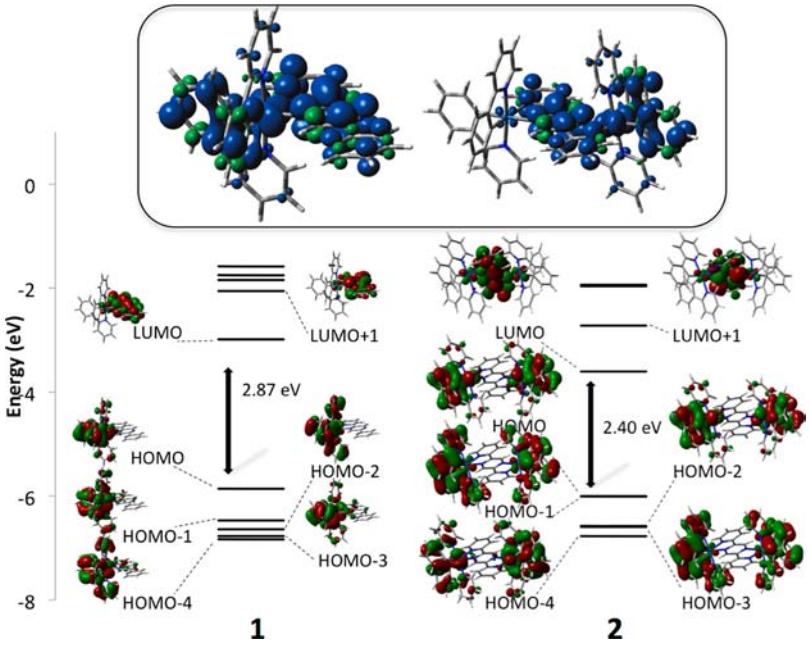

Figure 6. Calculated energy level scheme for the Kohn−Sham orbitals between HOMO−4 to LUMO+4 of **1** and **2** including contour plots (0.02 isovalue) of selected most relevant MOs and the associated DFT calculated HOMO−LUMO energy gap (in eV). Inset: spin density contour plots (0.002 isovalue) of the optimized T_1 state.

1 and **2**, it is not surprising that at RT the excited state of **2** is dominated by nonradiative decay, exhibiting nondetectable PL.

The emission lifetimes (τ_e) of **1** and **2** were also measured at RT (**1**) and low temperature (**1** and **2**). At RT, the emission of **1** is multiexponential and varies with wavelength. There is a shorter-lived species with an emission maximum around 700 nm, which dominates the steady state emission spectrum. There is also a much weaker, longer-lived species with an emission maximum around 600 nm. At 700 nm, the time-resolved emission decay is biexponential, with the largest contribution from the shorter lifetime (40 ns) and a small contribution from a longer and rather minor 240 ns component. At 600 nm, the time-resolved emission decay is best modeled as a sum of three exponential functions, with an additional 1250 ns component in addition to the 40 and 240 ns components observed at 700 nm. At 77 K the τ_e of **1** is significantly longer (3.6 μs) and is well modeled by a single exponential function. Surprisingly and unlike other dinuclear 2,5-dpp bridged systems, all of which contain Ru(II),[35,38,41] **2** has no detectable RT emission, but at 77 K it exhibits biexponential intensity decay kinetics with roughly two equivalent contributions corresponding to 360 and 930 ns excited state lifetimes. At present we can only speculate on this lack of PL at RT. Given the relatively rapid excited state decay in **1**, it is not surprising that the excited state decay of the red-shifted **2** is dominated by nonradiative decay, consistent with the energy gap law. From insights gleaned from the low temperature data, **2** is significantly quenched in comparison to **1**, thereby rationalizing the lack of detectable PL at RT. The transient absorption difference spectrum of **1** in RT acetonitrile was also recorded and is presented in Supporting Information, Figure S2. The transient absorption extracted single exponential excited state lifetime of 40 ns matches well with the measured PL lifetime of the major emissive component in **1** and does not indicate the presence of any longer-lived species. The shape of the difference spectrum is nearly identical to that seen in other $[Ir(ppy)_2(N^\wedge N)]^+$ CT complexes.[42] In particular, the sharp absorption feature at 400 nm has been assigned in the literature as an absorption of the polypyridyl radical anion, indicating that the lowest energy excited state is likely ^{3}MLCT in nature and localized on the 2,5-dpp ligand.[42] The combined data collected for **1** at RT strongly suggests that the CT excited state has a lifetime of 40 ns and the longer-lived residual components observed in the time-resolved PL intensity decays are not

dx.doi.org/10.1021/ic400478d | Inorg. Chem. 2013, 52, 8495−8504

representative of the excited state characteristics of this chromophore. Despite HPLC analyses indicating analytically pure samples and other corroborating compound characterization, the minor longer-lived species detected with transient PL is therefore most likely attributed to a minor luminescent impurity present in the sample, the origin of which is unknown. At low temperature where radiative decay dominates, only single exponential kinetics were observed in **1**, strongly supporting the notion that the longer-lived luminescent species observed at RT is/are irrelevant.

Computations. We have performed a combined DFT and TDDFT study to better understand the origin of the optoelectronic properties of **1** and **2**.[13a−c,14] We have previously shown that a similar computational methodology accurately predicts both ground and excited state properties for both mononuclear and dinuclear iridium complexes.[6m,23] Selected geometric parameters for the optimized ground and excited state geometries of **1** and **2** are reported in Supporting Information, Tables S2−S3. The computations accurately reproduce the principal structural features to within 3% relative error; however, the slight twisting of the distal pyridine ring in the crystal structure **1** (N_{pyz}-C_{pyz}-C_{py}-N_{py} torsion of 168.5) because of crystal packing forces, is not reproduced in the computations. No significant geometric changes are predicted to occur at the T_1 state.

Kohn−Sham energy diagrams for the five highest occupied and five lowest unoccupied MOs for **1** and **2** together with selected contour plots are shown in Figure 6 while important molecular orbital contributions for each of these MOs are summarized, respectively, in Supporting Information, Figures S4−S5. For each of the complexes, the HOMO is distributed approximately equally on the iridium and ppy ligands with only a 5% contribution arising from the 2,5-dpp. In **1**, the HOMO−2 through HOMO−4 electron distributions parallel that found for the HOMO while HOMO−1 is predominantly ppy-based (90%). In **2**, the HOMO−1 and HOMO−4 possess similar topologies to the HOMO while HOMO−2 and HOMO−3 are mostly localized on ppy (89 and 92%, respectively). The LUMO and LUMO+1 for each of the complexes are localized on the π^* orbitals of the 2,5-dpp (>90%). The LUMO+2 and LUMO+3 are concentrated mainly on the π^* orbitals of the ppy ligands while LUMO+4, like LUMO, is mostly $\pi^*_{2,5\text{-dpp}}$.

The HOMO and LUMO for **2** are both significantly stabilized compared to those in **1**. However, the larger stabilization of the LUMO results in a 470 meV decrease in the HOMO−LUMO gap, corroborating the observed electrochemical behavior. A similar degree of stabilization was observed upon homodimerization of $[Ir(ppy)_2(5\text{-ethynyl-bpy})]PF_6$.[6m] The LUMO+1 is also appreciably stabilized in **2**, which fits with the anodic shifting of the second reduction wave in **2** compared to **1**. The HOMO−1 in **2** is destabilized compared to HOMO−1 in **1**. The HOMO and HOMO−1 along with HOMO−2 and HOMO−3 are effectively isoenergetic with respect to each other.

To better comprehend the nature of the different absorption bands, TDDFT calculations of the 100 lowest-energy singlet−singlet and 5 lowest-energy singlet−triplet vertical transitions were performed. The most important low energy transitions are summarized in Table 3 while a comparison between the computed and experimental absorption spectra for **1** and **2** is shown in Figure 7 . The nature of the low energy absorption bands for each complex results from a series of ^{1}MLCT/^{1}LLCT transitions, consistent with the assignments for the experimental absorption spectra. For **1**, the intense bands at around 340 nm are the result of a mixed ^{1}LC transition localized on the 2,5-dpp ancillary ligand and a ^{1}LLCT transition (respectively, S_{12}, H-6→LUMO (82%), HOMO→L+4 (15%), f = 0.8855; S_{11}, H-6→LUMO (15%), HOMO→L+4 (83%), f = 0.1435). The intense higher energy absorption bands between 250 and 350 nm are dominated by mixed $^1LC_{ppy}$ and $^1LC_{2,5\text{-dpp}}$ transitions. A similar trend in assignments is observed for **2** wherein mixed ^{1}CT transitions define the spectral features below 350 nm and ^{1}LC transitions dominate at higher energies.

Table 3. Principal Theoretical Low Energy Electronic Transitions with Corresponding Oscillator Strengths (f) and Qualitative Assignments for 1 and 2

state	nature of transition (major contribution, %)[a,b]	primary character	ΔE (eV)	ΔE (nm)	oscillator strength (f)
		1			
S_1	HOMO→LUMO (98%),	MLCT/LLCT	2.21	560	0.0003
S_3	H-2→LUMO (26%), H-1→LUMO (68%)	MLCT/LLCT	2.96	419	0.0170
S_5	H-3→LUMO (69%), HOMO→L+1 (14%)	MLCT/LLCT/LC_{ppy}	3.17	391	0.0944
S_6	HOMO→L+2 (97%)	MLCT/LLCT	3.24	382	0.1108
T_1	HOMO→LUMO (97%)	MLCT/LLCT	2.18	568	0
		2			
S_1	HOMO→LUMO (99%),	LLCT/MLCT	1.77	701	0.0003
S_3	H-2→LUMO (95%)	LLCT/MLCT	2.46	504	0.0170
S_5	H-8→LUMO (23%), H-4→LUMO (71%)	MLCT/LLCT/	2.51	495	0.0944
S_6	H-6→LUMO (80%)	MLCT/LLCT	2.72	457	0.1108
T_1	HOMO→LUMO (98%)	MLCT/LLCT	1.74	712	0
T_2	H-1→LUMO (97%)	MLCT/LLCT	1.74	711	0

[a]H = HOMO; L = LUMO. [b]Major contributions defined as >10% contribution to the transition.

The geometry and energy of the T_1 state for each complex were fully optimized using unrestricted B3LYP (UB3LYP). The spin densities for the T_1 state are shown in the inset of Figure 6. For **1**, the spin density is distributed throughout the complex while for **2** one of the two iridium centers is bereft of spin density. However, a second isoenergetic T_2 state is predicted by TDDFT, which we hypothesize to contribute spin density to the second iridium center and its surrounding ligand sphere. From an evaluation of these spin density distributions along with the TDDFT calculations, the nature of the emission in each complex is attributed to a mixed ^{3}MLCT/LLCT state. The predicted emission energies computed as the difference between the T_1 and S_0 states at their respective optimized geometries, which approximates the $E_{0,0}$ emission band, are 602 and 767 nm, respectively, for **1** and **2**. These predictions match very well with the 77 K emission maximum observed for **1** and **2** at 589 and 715 nm, respectively. For both **1** and **2**, there is a substantial increase in the magnitude of the dipole moment in the T_1 state compared to the S_0 state of about 9 and 20 D, respectively. In particular, the orientation of the dipole in **2** remains unchanged in the excited state and is directed along an

dx.doi.org/10.1021/ic400478d | Inorg. Chem. 2013, 52, 8495−8504

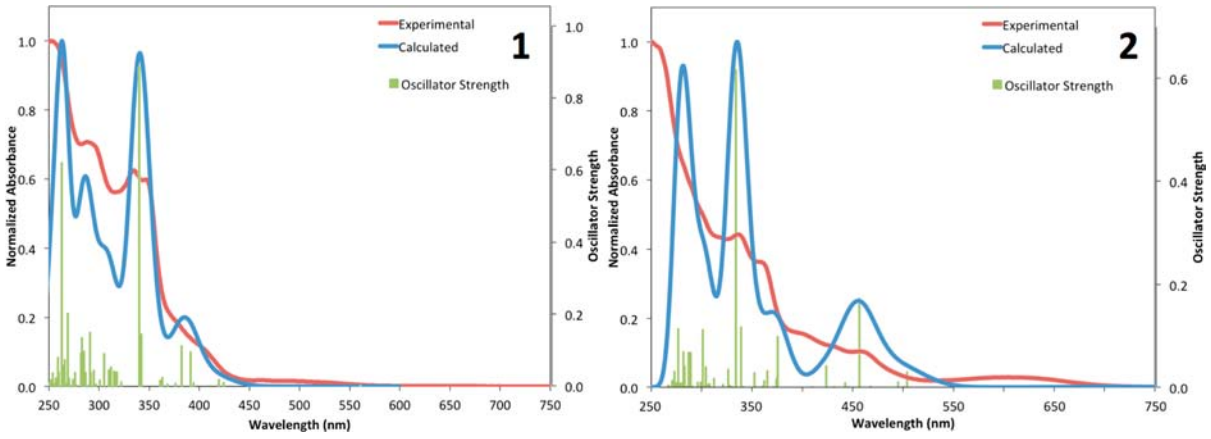

Figure 7. Experimental (red) and TDDFT simulated (blue) absorption spectra (fwhm 1000 cm^{-1}) of **1** (left) and **2** (right). The oscillator strengths (green) are represented by unbroadened vertical lines of the 100 lowest-energy calculated singlet−singlet transitions. UV−vis absorption spectra from 250 to 750 nm are shown.

axis linking the two iridium atoms, bifurcating the two nitrogen atoms of the pyrazine ring.

CONCLUSIONS

We presented the first examples of 2,5-dpp-containing iridium(III) complexes including their solid state structures. We showed that the 2,5-dpp ligand promotes a large red-shift in the RT emission spectrum for mononuclear complex **1**. The RT luminescence of dinuclear analogue **2** was unfortunately completely quenched. The deep-red emission and quasi-reversible electrochemical behavior in **1** makes it a promising candidate in red-emitting LEECs for flat panel lighting and visual displays.

ASSOCIATED CONTENT

Supporting Information

X-ray crystallographic data for **1** and **2** in CIF format. Tables of crystallographic refinement parameters and geometric features for **1** and **2**. X-ray packing diagram for **1**. ^{1}H NMR and ^{19}F NMR spectra for **1** and **2** and ^{1}H NMR and ^{13}C NMR spectra for 2,5-dpp. Supplementary photophysical and spectroscopic data for **1** and **2**. Selected data from TDDFT and DFT calculations. This material is available free of charge via the Internet at http://pubs.acs.org.

AUTHOR INFORMATION

Corresponding Author

*E-mail: eli.zysman-colman@usherbrooke.ca (E.Z.-C.), castell@bgsu.edu (F.N.C.).

Present Address

[§]School of Chemistry, University of St Andrews, St Andrews, Fife, UK, KY16 9ST, Fax: +44−1334 463808; Tel: +44−1334 463803; URL: http://www.zysman-colman.com.

Notes

The authors declare no competing financial interest.

ACKNOWLEDGMENTS

E.Z.-C. acknowledges CFI (Canadian Foundation for Innovation), NSERC (the National Sciences and Engineering Research Council of Canada), FQRNT (Le Fonds québécois de la recherche sur la nature et les technologies), and the Université de Sherbrooke for financial support.

REFERENCES

(1) (a) For recent reviews on LEECs see: Costa, R. D.; Ortí, E.; Bolink, H. J.; Monti, F.; Accorsi, G.; Armaroli, N. *Angew. Chem., Int. Ed.* **2012**, *51*, 8178. (b) Hu, T.; He, L.; Duan, L.; Qiu, Y. *J. Mater. Chem.* **2012**, *22*, 4206.

(2) (a) For recent reviews see: Lo, K. K.-W.; Louie, M.-W.; Zhang, K. Y. *Coord. Chem. Rev.* **2010**, *254*, 2603. (b) Baggaley, E.; Weinstein, J. A.; Williams, J. A. G. *Coord. Chem. Rev.* **2012**, *256*, 1762. (c) Zhao, Q.; Huang, C.; Li, F. *Chem. Soc. Rev.* **2011**, *40*, 2508.

(3) (a) Zhao, Q.; Li, F.; Huang, C. *Chem. Soc. Rev.* **2010**, *39*, 3007. (b) Lo, K. K.-W.; Li, S. P.-Y.; Zhang, K. Y. *New J. Chem.* **2011**, *35*, 265.

(4) (a) For recent reviews on solar fuels see: McDaniel, N. D.; Bernhard, S. *Dalton Trans.* **2010**, *39*, 10021. (b) Frischmann, P. D.; Mahata, K.; Wurthner, F. *Chem. Soc. Rev.* **2013**, *42*, 1847.

(5) (a) For a recent review on photocatalysis of organic substrates see: Narayanam, J. M. R.; Stephenson, C. R. J. *Chem. Soc. Rev.* **2011**, *40*, 102. (b) Tucker, J. W.; Stephenson, C. R. J. *J. Org. Chem.* **2012**, *77*, 1617. (c) Shi, L.; Xia, W. *Chem. Soc. Rev.* **2012**, *41*, 7687.

(6) (a) Neve, F.; Crispini, A.; Serroni, S.; Loiseau, F.; Campagna, S. *Inorg. Chem.* **2001**, *40*, 1093. (b) Plummer, E. A.; Hofstraat, J. W.; De Cola, L. *Dalton Trans.* **2003**, 2080. (c) Lafolet, F.; Welter, S.; Popovic, Z.; De Cola, L. *J. Mater. Chem.* **2005**, *15*, 2820. (d) Auffrant, A.; Barbieri, A.; Barigelletti, F.; Lacour, J.; Mobian, P.; Collin, J.-P.; Sauvage, J.-P.; Ventura, B. *Inorg. Chem.* **2007**, *46*, 6911. (e) Costa, R. D.; Fernández, G.; Sánchez, L.; Martín, N.; Ortí, E.; Bolink, H. J. *Chem.—Eur. J.* **2010**, *16*, 9855. (f) Chandrasekhar, V.; Hajra, T.; Bera, J. K.; Rahaman, S. M. W.; Satumtira, N.; Elbjeirami, O.; Omary, M. A. *Inorg. Chem.* **2012**, *51*, 1319. (g) Chandrasekhar, V.; Wahidur Rahaman, S. M.; Hajra, T.; Das, D.; Ghatak, T.; Rafiq, S.; Sen, P.; Bera, J. K. *Chem. Commun.* **2011**, *47*, 10836. (h) Hajra, T.; Bera, J. K.; Chandrasekhar, V. *Inorg. Chim. Acta* **2011**, *372*, 53. (i) Cavazzini, M.; Pastorelli, P.; Quici, S.; Loiseau, F.; Campagna, S. *Chem. Commun.* **2005**, 5266. (j) Whittle, V. L.; Williams, J. A. G. *Inorg. Chem.* **2008**, *47*, 6596. (k) Whittle, V. L.; Williams, J. A. G. *Dalton Trans.* **2009**, 3929. (l) Auffrant, A.; Barbieri, A.; Barigelletti, F.; Collin, J.-P.; Flamigni, L.; Sabatini, C.; Sauvage, J.-P. *Inorg. Chem.* **2006**, *45*, 10990. (m) Soliman, A. M.; Fortin, D.; Harvey, P. D.; Zysman-Colman, E. *Dalton Trans.* **2012**, *41*, 9382. (n) Xu, W.-J.; Liu, S.-J.; Zhao, X.; Zhao, N.; Liu, Z.-Q.; Xu, H.; Liang, H.; Zhao, Q.; Yu, X.-Q.; Huang, W. *Chem.—Eur. J.* **2013**, *19*, 621. (o) Osío Barcina, J.; Herrero-García, N.; Cucinotta, F.; De Cola, L.; Contreras-Carballada, P.; Williams, R. M.; Guerrero-Martínez, A. *Chem.—Eur. J.* **2010**, *16*, 6033. (p) Pandrala, M.; Li, F.; Feterl, M.; Mulyana, Y.; Warner, J. M.; Wallace, L.; Keene, F. R.; Collins, J. G. *Dalton Trans.* **2013**, *42*, 4686−4694. (q) Li, G.; Chen, Y.; Wu, J.; Ji, L.; Chao, H. *Chem. Commun.* **2013**, *49*, 2040. (r) Baranoff, E.; Orselli, E.; Allouche, L.; Di Censo, D.; Scopelliti, R.; Gratzel, M.; Nazeeruddin, M. K. *Chem. Commun.* **2011**, *47*, 2799. (s) Chepelin, O.; Ujma, J.; Wu, X.; Slawin, A. M. Z.; Pitak, M. B.; Coles, S. J.; Michel, J.;

Jones, A. C.; Barran, P. E.; Lusby, P. J. *J. Am. Chem. Soc.* **2012**, *134*, 19334. (t) McCusker, C. E.; Hablot, D.; Ziessel, R.; Castellano, F. N. *Inorg. Chem.* **2012**, *51*, 7957.
(7) (a) For original report of the synthesis of 2,5-dpp see: Case, F. H.; Koft, E. *J. Am. Chem. Soc.* **1959**, *81*, 905. (b) For earliest reports of the use of 2,5-dpp as a ligand with Ru(II) see: Ernst, S. D.; Kaim, W. *Inorg. Chem.* **1989**, *28*, 1520. (c) Campagna, S.; Denti, G.; De Rosa, G.; Sabatino, L.; Ciano, M.; Balzani, V. *Inorg. Chem.* **1989**, *28*, 2565.
(8) (a) Lincker, F.; Kreher, D.; Attias, A.-J.; Do, J.; Kim, E.; Hapiot, P.; Lemaître, N.; Geffroy, B.; Ulrich, G.; Ziessel, R. *Inorg. Chem.* **2010**, *49*, 3991. (b) Dürr, H.; Schwarz, R.; Andreis, C.; Willner, I. *J. Am. Chem. Soc.* **1993**, *115*, 12362.
(9) Neels, A.; Stoeckli-Evans, H. *Inorg. Chem.* **1999**, *38*, 6164.
(10) Ishida, H.; Tobita, S.; Hasegawa, Y.; Katoh, R.; Nozaki, K. *Coord. Chem. Rev.* **2010**, *254*, 2449.
(11) Pavlishchuk, V. V.; Addison, A. W. *Inorg. Chim. Acta* **2000**, *298*, 97.
(12) Frisch, M. J.; Trucks, G. W.; Schlegel, H. B.; Scuseria, G. E.; Robb, M. A.; Cheeseman, J. R.; Scalmani, G.; Barone, V.; Mennucci, B.; Petersson, G. A.; Nakatsuji, H.; Caricato, M.; Li, X.; Hratchian, H. P.; Izmaylov, A. F.; Bloino, J.; Zheng, G.; Sonnenberg, J. L.; Hada, M.; Ehara, M.; Toyota, K.; Fukuda, R.; Hasegawa, J.; Ishida, M.; Nakajima, T.; Honda, Y.; Kitao, O.; Nakai, H.; Vreven, T.; Montgomery, J., J. A.; Peralta, J. E.; Ogliaro, F.; Bearpark, M.; Heyd, J. J.; Brothers, E.; Kudin, K. N.; Staroverov, V. N.; Kobayashi, R.; Normand, J.; Raghavachari, K.; Rendell, A.; Burant, J. C.; Iyengar, S. S.; Tomasi, J.; Cossi, M.; Rega, N.; Millam, J. M.; Klene, M.; Knox, J. E.; Cross, J. B.; Bakken, V.; Adamo, C.; Jaramillo, J.; Gomperts, R.; Stratmann, R. E.; Yazyev, O.; Austin, A. J.; Cammi, R.; Pomelli, C.; Ochterski, J. W.; Martin, R. L.; Morokuma, K.; Zakrzewski, V. G.; Voth, G. A.; Salvador, P.; Dannenberg, J. J.; Dapprich, S.; Daniels, A. D.; Farkas, Ö.; Foresman, J. B.; Ortiz, J. V.; Cioslowski, J.; Fox, D. J. *Gaussian09*, 7.0 ed.; Wallingford, CT, 2009.
(13) (a) Hohenberg, P.; Kohn, W. *Phys. Rev.* **1964**, *B136*, 864. (b) Kohn, W.; Sham, L. *J. Phys. Rev.* **1965**, *A140*, 1133. (c) In *The Challenge of d and f Electrons*; Salahub, D. R., Zerner, M. C., Eds.; American Chemical Society: Washington, DC, 1989; (d) Parr, R. G.; Yang, W. *Density-functional theory of atoms and molecules*; Oxford University Press: Oxford, U.K., 1989.
(14) (a) Stratmann, R. E.; Scuseria, G. E.; Frisch, M. J. *J. Chem. Phys.* **1998**, *109*, 8218. (b) Bauernschmitt, R.; Ahlrichs, R. *Chem. Phys. Lett.* **1996**, *256*, 454. (c) Casida, M. E.; Jamorski, C.; Casida, K. C.; Salahub, D. R. *J. Chem. Phys.* **1998**, *108*, 4439.
(15) (a) Becke, A. D. *J. Chem. Phys.* **1993**, *98*, 5648. (b) Lee, C.; Yang, W.; Parr, R. G. *Phys. Rev. B* **1988**, *37*, 785. (c) Miehlich, B.; Savin, A.; Stoll, H.; Preuss, H. *Chem. Phys. Lett.* **1989**, *157*, 200.
(16) Rassolov, V. A.; Pople, J. A.; Ratner, M. A.; Windus, T. L. *J. Chem. Phys.* **1998**, *109*, 1223.
(17) (a) Binkley, J. S.; Pople, J. A.; Hehre, W. J. *J. Am. Chem. Soc.* **1980**, *102*, 939. (b) Gordon, M. S.; Binkley, J. S.; Pople, J. A.; Pietro, W. J.; Hehre, W. J. *J. Am. Chem. Soc.* **1982**, *104*, 2797. (c) Pietro, W. J.; Francl, M. M.; Hehre, W. J.; Defrees, D. J.; Pople, J. A.; Binkley, J. S. *J. Am. Chem. Soc.* **1982**, *104*, 5039. (d) Dobbs, K. D.; Hehre, W. J. *J. Comput. Chem.* **1986**, *7*, 359. (e) Dobbs, K. D.; Hehre, W. J. *J. Comput. Chem.* **1987**, *8*, 861. (f) Dobbs, K. D.; Hehre, W. J. *J. Comput. Chem.* **1987**, *8*, 880.
(18) (a) Stevens, W. J.; Basch, W. J.; Krauss, M. *J. Chem. Phys.* **1984**, *81*, 6026. (b) Stevens, W. J.; Krauss, M.; Basch, H.; Jasien, P. G. *Can. J. Chem.* **1992**, *70*, 612. (c) Cundari, T. R.; Stevens, W. J. *J. Chem. Phys.* **1993**, *98*, 5555.
(19) (a) Ladouceur, S.; Fortin, D.; Zysman-Colman, E. *Inorg. Chem.* **2010**, *49*, 5625. (b) Lowry, M. S.; Hudson, W. R.; Pascal, R. A., Jr.; Bernhard, S. *J. Am. Chem. Soc.* **2004**, *126*, 14129.
(20) O'Boyle, N. M. *GaussSum 2.0*; Dublin City University: Dubin Ireland, 2006; available at http://gausssum.sf.net.
(21) Tomasi, J.; Mennucci, B.; Cammi, R. *Chem. Rev.* **2005**, *105*, 2999.
(22) (a) Escuer, A.; Comas, T.; Vicente, R.; Ribas, J. *Transition Met. Chem.* **1993**, *18*, 42. (b) Yuste, C.; Bentama, A.; Stiriba, S.-E.; Armentano, D.; De Munno, G.; Lloret, F.; Julve, M. *Dalton Trans.* **2007**, 5190. (c) Neels, A.; Stoeckli-Evans, H. *Chimia* **1993**, *47*, 198.
(23) Ladouceur, S.; Fortin, D.; Zysman-Colman, E. *Inorg. Chem.* **2011**, *50*, 11514.
(24) Costa, R. D.; Ortì, E.; Bolink, H. J.; Graber, S.; Schaffner, S.; Neuburger, M.; Housecroft, C. E.; Constable, E. C. *Adv. Funct. Mater.* **2009**, *19*, 3456.
(25) Constable, E. C.; Eriksson, H.; Housecroft, C. E.; Kariuki, B. M.; Nordlander, E.; Olsson, J. *Inorg. Chem. Commun.* **2001**, *4*, 749.
(26) Bettington, S.; Tavasli, M.; Bryce, M. R.; Batsanov, A. S.; Thompson, A. L.; Attar, H. A. A.; Dias, F. B.; Monkman, A. P. *J. Mater. Chem.* **2006**, *16*, 1046.
(27) (a) M'Hamedi, A.; Batsanov, A. S.; Fox, M. A.; Bryce, M. R.; Abdullah, K.; Al-Attar, H. A.; Monkman, A. P. *J. Mater. Chem.* **2012**, *22*, 13529. (b) Chandrasekhar, V.; Mahanti, B.; Bandipalli, P.; Bhanuprakash, K. *Inorg. Chem.* **2012**, *51*, 10536. (c) Davies, D. L.; Lowe, M. P.; Ryder, K. S.; Singh, K.; Singh, S. *Dalton Trans.* **2011**, *40*, 1028. (d) Chen, L.-Q.; Yang, C.-L.; Qin, J.-G. *Acta Crystallogr., Sect. C: Cryst. Struct. Commun.* **2005**, *61*, m513. (e) Chen, L.; Yang, C.; Li, M.; Qin, J.; Gao, J.; You, H.; Ma, D. *Cryst. Growth Des.* **2006**, *7*, 39. (f) Krisyuk, V.; Turgambaeva, A.; Lee, J.; Rhee, S.-W. *Transition Met. Chem.* **2005**, *30*, 786. (g) Jiménez, M. V.; Sola, E.; López, J. A.; Lahoz, F. J.; Oro, L. A. *Chem.—Eur. J.* **1998**, *4*, 1398. (h) Garces, F. O.; Dedeian, K.; Keder, N. L.; Watts, R. J. *Acta Crystallogr., Sect. C: Cryst. Struct. Commun.* **1993**, *49*, 1117.
(28) Andreiadis, E. S.; Imbert, D.; Pécaut, J.; Calborean, A.; Ciofini, I.; Adamo, C.; Demadrille, R.; Mazzanti, M. *Inorg. Chem.* **2011**, *50*, 8197.
(29) Cardona, C. M.; Li, W.; Kaifer, A. E.; Stockdale, D.; Bazan, G. C. *Adv. Mater.* **2011**, *23*, 2367.
(30) Singh Bindra, G.; Schulz, M.; Paul, A.; Soman, S.; Groarke, R.; Inglis, J.; Pryce, M. T.; Browne, W. R.; Rau, S.; Maclean, B. J.; Vos, J. G. *Dalton Trans.* **2011**, *40*, 10812.
(31) D'Alessandro, D. M.; Keene, F. R. *New J. Chem.* **2006**, *30*, 228.
(32) de Cola, L.; Balzani, V.; Barigelletti, F.; Flamigni, L.; Belser, P.; Bernhard, S. *Recl. Trav. Chim. Pays-Bas* **1995**, *114*, 534.
(33) (a) Van Diemen, J. H.; Hage, R.; Haasnoot, J. G.; Lempers, H. E. B.; Reedijk, J.; Vos, J. G.; De Cola, L.; Barigelletti, F.; Balzani, V. *Inorg. Chem.* **1992**, *31*, 3518. (b) Carlson, G. A.; Djurovich, P. I.; Watts, R. J. *Inorg. Chem.* **1993**, *32*, 4483.
(34) Shin, C. H.; Huh, J. O.; Baek, S. J.; Kim, S. K.; Lee, M. H.; Do, Y. *Eur. J. Inorg. Chem.* **2010**, *2010*, 3642.
(35) Denti, G.; Campagna, S.; Sabatino, L.; Serroni, S.; Ciano, M.; Balzani, V. *Inorg. Chem.* **1990**, *29*, 4750.
(36) Al-Anber, M.; Vatsadze, S.; Holze, R.; Lang, H.; Thiel, W. R. *Dalton Trans.* **2005**, 3632.
(37) Soman, S.; Singh Bindra, G.; Paul, A.; Groarke, R.; Manton, J. C.; Connaughton, F. M.; Schulz, M.; Dini, D.; Long, C.; Pryce, M. T.; Vos, J. G. *Dalton Trans.* **2012**, *41*, 12678.
(38) Schulz, M.; Hirschmann, J.; Draksharapu, A.; Singh Bindra, G.; Soman, S.; Paul, A.; Groarke, R.; Pryce, M. T.; Rau, S.; Browne, W. R.; Vos, J. G. *Dalton Trans.* **2011**, *40*, 10545.
(39) Crosby, G. A.; Watts, R. J.; Carstens, D. H. W. *Science* **1970**, *170*, 1195.
(40) (a) He, L.; Qiao, J.; Duan, L.; Dong, G.; Zhang, D.; Wang, L.; Qiu, Y. *Adv. Funct. Mater.* **2009**, *19*, 2950. (b) Medina-Castillo, A. L.; Fernandez-Sanchez, J. F.; Klein, C.; Nazeeruddin, M. K.; Segura-Carretero, A.; Fernandez-Gutierrez, A.; Graetzel, M.; Spichiger-Keller, U. E. *Analyst* **2007**, *132*, 929. (c) Costa, R. D.; Cespedes-Guirao, F. J.; Orti, E.; Bolink, H. J.; Gierschner, J.; Fernandez-Lazaro, F.; Sastre-Santos, A. *Chem. Commun.* **2009**, 3886. (d) Lo, K. K.-W.; Chung, C.-K.; Zhu, N. *Chem.—Eur. J.* **2006**, *12*, 1500. (e) Sun, J.; Wu, W.; Zhao, J. *Chem.—Eur. J.* **2012**, *18*, 8100. (f) Hanss, D.; Freys, J. C.; Bernardinelli, G.; Wenger, O. S. *Eur. J. Inorg. Chem.* **2009**, *2009*, 4850. (g) Neve, F.; Crispini, A.; Campagna, S.; Serroni, S. *Inorg. Chem.* **1999**, *38*, 2250. (h) Shao, F.; Elias, B.; Lu, W.; Barton, J. K. *Inorg. Chem.* **2007**, *46*, 10187. (i) Zhang, K. Y.; Lo, K. K.-W. *Inorg. Chem.* **2009**, *48*, 6011. (j) Rachford, A. A.; Ziessel, R.; Bura, T.; Retailleau, P.; Castellano, F. N. *Inorg. Chem.* **2010**, *49*, 3730. (k) Aubert, V.;

Ordronneau, L.; Escadeillas, M.; Williams, J. A. G.; Boucekkine, A.; Coulaud, E.; Dragonetti, C.; Righetto, S.; Roberto, D.; Ugo, R.; Valore, A.; Singh, A.; Zyss, J.; Ledoux-Rak, I.; Le Bozec, H.; Guerchais, V. r. *Inorg. Chem.* **2011**, *50*, 5027. (l) The emission was reported in DCM. Shavaleev, N. M.; Scopelliti, R.; Grätzel, M.; Nazeeruddin, M. K. *Inorg. Chim. Acta* **2013**, *394*, 295. (m) The emission was reported in DCM. Su, H.-C.; Chen, H.-F.; Fang, F.-C.; Liu, C.-C.; Wu, C.-C.; Wong, K.-T.; Liu, Y.-H.; Peng, S.-M. *J. Am. Chem. Soc.* **2008**, *130*, 3413. (n) The emission was measured in 2-MeTHF. Cunningham, G. B.; Li, Y.; Liu, S.; Schanze, K. S. *J. Phys. Chem. B* **2003**, *107*, 12569. (o) Kim, K.-Y.; Farley, R. T.; Schanze, K. S. *J. Phys. Chem. B* **2006**, *110*, 17302. (p) Neve, F.; LaDeda, M.; Crispini, A.; Bellusci, A.; Puntoriero, F.; Campagna, S. *Organometallics* **2004**, *23*, 5856. (q) Rodriguez-Redondo, J. L.; Costa, R. D.; Orti, E.; Sastre-Santos, A.; Bolink, H. J.; Fernandez-Lazaro, F. *Dalton Trans.* **2009**, *0*, 9787.

(41) (a) Juris, A.; Balzani, V.; Campagna, S.; Denti, G.; Serroni, S.; Frei, G.; Guedel, H. U. *Inorg. Chem.* **1994**, *33*, 1491. (b) Sommovigo, M.; Denti, G.; Serroni, S.; Campagna, S.; Mingazzini, C.; Mariotti, C.; Juris, A. *Inorg. Chem.* **2001**, *40*, 3318. (c) Tsubomura, T.; Enoto, S.; Endo, S.; Tamane, T.; Matsumoto, K.; Tsukuda, T. *Inorg. Chem.* **2005**, *44*, 6373. (d) Baudin, H. B.; Davidsson, J.; Serroni, S.; Juris, A.; Balzani, V.; Campagna, S.; Hammarström, L. *J. Phys. Chem. A* **2002**, *106*, 4312.

(42) Ichimura, K.; Kobayashi, T.; King, K. A.; Watts, R. J. *J. Phys. Chem.* **1987**, *91*, 6104.